


New Aspects of Exponential Asymptotics in Multiple-Scale Nonlinear Wave Problems

By Sean D. Nixon, T. R. Akylas, and Jianke Yang 

It is known that standard multiple-scale perturbation techniques fail to pinpoint the soliton solution branches that bifurcate at edges of bandgaps in periodic media, owing to the appearance of exponentially small growing wave tails when the soliton's envelope is not properly positioned. When the bifurcation is from a single wave mode of a band edge, this difficulty has been handled in recent work by computing these tails via an exponential asymptotics technique in the wave number domain. However, the same approach is not directly applicable to the bifurcation of solitons near the opening of a bandgap, where wave modes from two nearby band edges interact with each other. Here, we discuss two nontrivial extensions of the exponential asymptotics technique that enable resolving this issue. For simplicity, the analysis focuses on two model problems, namely, a steady-state forced Korteweg–de Vries equation and a steady-state forced nonlinear Schrödinger equation, with the precise form of forcing and balance between nonlinear and dispersive terms chosen so as to mimic the situation encountered in the bifurcation of solitons near a bandgap opening. Our analysis exhibits a number of new features that are significantly different from previous exponential asymptotics procedures, such as the treatments when the nonlinearity dominates dispersion and when the decay rates of the Fourier-transformed solution are asymmetric. In addition, the analysis reveals new, and in some cases rather unexpected, functional forms

The late Professor David Benney made truly seminal contributions to singular perturbation methods for nonlinear wave problems. As mentor, teacher, and friend, he left an everlasting imprint on our scientific thinking and professional development. This paper in his memory is a small token of gratitude and respect.

Address for correspondence: Prof. J. Yang, Department of Mathematics and Statistics, University of Vermont, 16 Colchester Avenue, Burlington, VT 05401; e-mail: jxyang@uvm.edu

for exponentially small wave tails, which are also confirmed by numerical results.

1. Introduction

In a 1977 paper on nonlinear interactions between long and short waves [1], David Benney commented that “Theoretical progress in fluid mechanics is sometimes initiated by making use of the fact that there may be distinct scales in the problem.” Indeed, exploiting the presence of disparate length and/or time scales forms the basis of boundary-layer theory and the method of multiple scales, the two most well-known singular perturbation techniques in applied mathematics. Benney, in particular, pioneered the use of multiple-scale techniques for deriving evolution equations, most notably the nonlinear Schrödinger (NLS) equation and the Benney–Roskes–Davey–Stewartson equations, in the study of nonlinear waves and fluid flows [2–4]. These evolution equations turn out to be fundamental to nonlinear science and find applications in various other fields, including nonlinear optics and Bose–Einstein condensates [5–8].

In spite of numerous successes, however, it is now recognized that multiple-scale asymptotic techniques also suffer certain limitations. Specifically, in the context of solitary wave propagation, these shortcomings manifest in: (i) the appearance of short-scale oscillations at the tails of Korteweg–de Vries (KdV) and NLS solitary waves in the presence of a higher order dispersion perturbation, which cannot be captured at any order by standard multiple-scale expansions [9–14]; and (ii) the bifurcation of solitary wave packets at edges of the linear continuous-wave spectrum, where standard two-scale perturbation expansions fail to pinpoint the proper bifurcating solution branches [15]. Physically, the first of these difficulties is relevant to gravity–capillary solitary waves in shallow water [16–18] and internal gravity waves in a stratified fluid layer [19]; the second arises in the bifurcation of gravity–capillary solitary waves on deep water [20] as well as gap solitons from Bloch band edges in periodic media [21–25].

In both (i) and (ii) above, standard multiscale perturbation techniques assume from the outset complete separation of length scales, thus ignoring the presence of exponentially small long–short wave coupling that lies beyond all orders of the perturbation series expansion. In the case of KdV and NLS solitary waves with short oscillatory tails, these tails arise due to their coupling with the copropagating main solitary-wave core and have exponentially small amplitude relative to the solitary-wave core [9–14]. In the bifurcation of solitary wave packets from edges of the continuous-wave

spectrum, however, the wave packets develop growing tails of exponentially small amplitude due to coupling of the wave envelope with the underlying periodic carrier; these growing tails vanish only if the envelope is suitably placed relative to the carrier [15, 21–25].

The generation of exponentially small short-scale tails by long-wave cores can be captured by carrying the standard perturbation expansions beyond all orders. The application of such exponential asymptotics perturbation techniques to multiscale nonlinear wave problems has attracted considerable interest in the last 30 years, and two separate methods of attack have emerged (see [7, 26] and references therein). The first method focuses on singularities of the standard expansions in the complex plane, where these “outer” expansions become disordered and rescaling becomes necessary. Thus, in the vicinity of each singularity, an “inner” problem is formulated, which, importantly, contains information on the long–short wave coupling. Solving this problem subject to appropriate inner–outer matching conditions for the singularity then enables the calculation of the exponentially small wave tail.

The second approach, proposed in [27], recognizes that the short-scale wave tails in the physical domain are tied to simple poles on (or very close to) the real axis in the Fourier (wave number) domain. So, the analysis focuses on computing the residues of these simple poles, which have exponentially small amplitude. Unlike the standard expansion in the physical domain, which shows no sign of tails at any order, the analogous expansion in the Fourier domain becomes disordered at large wave numbers, where the poles responsible for the tails reside. This nonuniformity is then handled by introducing a “stretched” wave number variable. Thus, by working in the wave number domain, it is possible to use a standard two-scale perturbation procedure for obtaining a uniformly valid expression for the Fourier transform, and thereby the pole residues that furnish the tail amplitude upon inversion of the transform.

For KdV solitary waves with oscillatory tails and related problems, the wave number approach yields a uniformly valid approximate integral equation for the Fourier transform, which readily furnishes the desired simple-pole residues [27]. In other situations, however, it turns out that this leading-order integral equation is not valid very close to the poles; rather, it serves as an “outer” equation that has to be supplemented with an “inner” integral equation in order to compute the pole residues. This significant complication, first brought out in [27] using a steady-state forced KdV equation as a model problem arises in the bifurcation of solitary gravity–capillary wave packets at the minimum phase speed on deep water [15], as well as gap solitons bifurcating from the edge of a bandgap in periodic media [22, 24, 25].

In this paper, we discuss two further nontrivial extensions of the wave number approach for computing exponentially small wave tails. The original motivation comes from the need to understand the bifurcation of gap solitons near the opening of a bandgap in periodic media. Specific examples include the NLS equation in the presence of a weak periodic potential, a mathematical model for Bose–Einstein condensates loaded in optical lattices [8, 28] and laser beam transmission in photonic lattices [7], as well as surface waves over a bottom with small-amplitude periodic corrugations [29]. In this setting, the expansion of the Fourier transform again becomes disordered for large wave numbers, suggesting the presence of poles whose residues give the exponentially small amplitude of the growing tails; moreover, the reduced integral equations near the poles and away from them are different, requiring the matching between those “inner” and “outer” solutions. However, the previous exponential asymptotic technique, as was successfully developed in [22, 24, 25] for the bifurcation of gap solitons near edges of finite bandgaps, is not directly applicable. The reason is that near a bandgap opening, wave modes from two nearby band edges interact with each other. This mode coupling creates two serious complications for the application of exponential asymptotics in the wave number domain. The first one is that the nonlinear terms here make a stronger contribution to the disordering of the Fourier-transformed solution than the dispersive terms. As a result, the location of the poles, which is fixed by linear dispersive effects, is on an even longer wave number scale than the disordering scale of the Fourier transform. The second complication is that the Fourier-transformed solution here features different decay rates in the positive and negative wave number directions, making the derivation of the inner and outer integral equations, as well as the calculation of the pole residues, significantly more involved than previous cases.

Here, working in the same spirit as [27], we tackle these issues using two simple model problems, namely, a steady-state forced KdV equation and a steady-state forced NLS equation. In each of these models, the precise form of forcing and balance between nonlinear and dispersive terms are chosen so as to mimic the situation encountered in the bifurcation of gap solitons near a bandgap opening. On the issue of nonlinearity dominating dispersion, we show that both the inner and outer integral equations in the exponential asymptotics procedure become ϵ -dependent, where ϵ is the short scale of oscillatory tails. As a result, the induced exponentially small tail has a rather intricate dependence on ϵ . On the issue of asymmetric decay rates in the Fourier transform, we show that this asymmetry gives rise to asymmetric residues of the poles, which necessitates two coupled integral equations in the inner and outer regions in order to compute these residues and thereby the generated tails. In all cases, our analytical formulas for the generated tails are verified by direct numerical results.

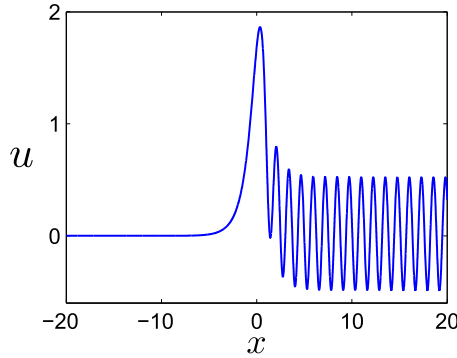


Figure 1. Solution $u(x)$ to Eq. (1) subject to the upstream condition (2) with $\epsilon = 0.2$ and $\sigma = 0.5$.

2. Oscillatory tails in a steady-state forced KdV equation

In our first example, we consider the steady-state KdV equation with a localized forcing:

$$\epsilon^2 u_{xx} + u - \sigma \sqrt{\epsilon} u^2 = \operatorname{sech} x, \quad (1)$$

subject to the boundary condition

$$u(x) \rightarrow 0, \quad x \rightarrow -\infty. \quad (2)$$

Here, $0 < \epsilon \ll 1$ and σ is a free positive constant. This problem arises when one considers the KdV equation under a moving slowly varying low-amplitude forcing. Looking for steady states (relative to the moving force) and after variable normalization, one gets Eq. (1). The boundary condition (2) is the appropriate radiation condition for this steady state because the resonant radiation has group velocity greater than the speed of the moving force and thus appears only ahead of the forcing. This model problem has been analyzed in [27,30], but with a different scaling ($\sigma = \sqrt{\epsilon}$) of the nonlinear term. Now, the $\sigma = O(1)$ scaling makes the nonlinear term stronger, which has important ramifications for the ensuing analysis.

Solutions to this problem, which decay to zero upstream ($x \rightarrow -\infty$), will develop short-scale oscillatory tails downstream ($x \rightarrow \infty$). An example is shown in Fig. 1, where the parameters are chosen as $\epsilon = 0.2$ and $\sigma = 0.5$. These oscillatory tails are induced by a resonance between the forcing term $\operatorname{sech} x$ and the linear oscillatory waves at large wave numbers $k = \pm 1/\epsilon$. When $\epsilon \rightarrow 0$, the amplitudes of these oscillatory tails are exponentially small in ϵ because the spectral amplitudes of the forcing term at the resonant wave numbers $k = \pm 1/\epsilon$ are exponentially small. For this reason, these tails cannot be detected by standard perturbation expansions in powers of ϵ . Instead, exponential asymptotics is needed.

The key novel feature here is the imbalance between the nonlinear and dispersive terms. As nonlinearity dominates dispersion, the disordering of the asymptotic expansion in the Fourier domain is prominently associated with the nonlinear effects. However, resonance that gives rise to the oscillatory tails is a linear effect, and the location of the related poles in the Fourier domain is dictated by the dispersive term. This incongruity leads to a novel scenario in which the poles appear on a longer wave number scale than the disordering scale of the Fourier-transform expansion. In this section, we develop the analysis to handle this situation and calculate the more complex ϵ -dependency of the exponentially small tails.

Looking for a solution in terms of a regular perturbation expansion in ϵ yields

$$u(x) \sim \operatorname{sech} x + \sqrt{\epsilon} \sigma \operatorname{sech}^2 x + 2\epsilon \sigma^2 \operatorname{sech}^3 x + \dots, \quad (3)$$

which has the Fourier transform

$$\hat{u}(k) \sim \frac{1}{2} [1 + \epsilon \sigma^2 (1 + k^2) + \dots] \operatorname{sech} \frac{\pi k}{2} + \frac{1}{2} \sigma \sqrt{\epsilon} k \operatorname{csch} \frac{\pi k}{2} + \dots \quad (4)$$

Here, the Fourier transform is defined as

$$\hat{u}(k) = \frac{1}{2\pi} \int_{-\infty}^{\infty} u(x) e^{-ikx} dx. \quad (5)$$

Note that the leading order secular terms above come solely from the nonlinearity. In the Fourier domain, this expansion becomes disordered at $\kappa \equiv \epsilon^{1/2} k = O(1)$, and suggests the following form of the solution for $k \gg 1$:

$$\hat{u}(k) = \frac{1}{2} U(\kappa) \operatorname{sech} \frac{\pi k}{2}, \quad (6)$$

where

$$U(\kappa) \rightarrow 1 \text{ as } \kappa \rightarrow 0, \epsilon \rightarrow 0. \quad (7)$$

Here, the function $U(\kappa)$ depends explicitly on ϵ as well, and this ϵ dependence is suppressed for notational simplicity. Substituting this transformation back in Eq. (1), the equation for $U(\kappa)$ is found to be

$$(1 - \epsilon \kappa^2) U(\kappa) - \frac{1}{2} \sigma \cosh \frac{\pi \kappa}{2\sqrt{\epsilon}} \int_{-\infty}^{\infty} \frac{U(\lambda) U(\kappa - \lambda)}{\cosh \frac{\pi \lambda}{2\sqrt{\epsilon}} \cosh \frac{\pi(\kappa - \lambda)}{2\sqrt{\epsilon}}} d\lambda = 1. \quad (8)$$

Looking at the linear terms, we readily see that $U(\kappa)$ has a singularity at $\kappa_0 = \epsilon^{-1/2}$. For the scaling used in [27] and other previous works, the location of the pole has been independent of ϵ once moving to the long wave number scaling κ . As we show in the following analysis, here, not only does the location of the pole depend on ϵ , but also the residue of the pole varies with ϵ .

2.1. The outer equation

For $0 < \kappa < \kappa_0$, the integral in Eq. (8) can be simplified. Indeed, on the integration interval $0 < \lambda < \kappa$, the denominator is approximately a constant $\exp(\pi\kappa/2\sqrt{\epsilon})/4$; while outside the interval $0 < \lambda < \kappa$, it is exponentially large, thus making a negligible contribution to the integral. Under this simplification, the reduced outer equation is

$$(1 - \epsilon\kappa^2)U - \sigma \int_0^\kappa U(\lambda)U(\kappa - \lambda)d\lambda = 1, \tag{9}$$

which proves to be asymptotically accurate (for small ϵ) over the entire κ interval of $0 < \kappa < \kappa_0$. It is important to note here that the error in the approximation of the convolution comes mainly from the two edges of the λ interval $[0, \kappa]$ and is $O(\sqrt{\epsilon})$. In contrast, the $O(\epsilon)$ contribution in the linear terms increases to $O(1)$ as $\kappa \rightarrow \kappa_0$. For this reason, the $O(\epsilon)$ linear term must be kept to maintain the validity of Eq. (9) for $0 < \kappa < \kappa_0$.

In this outer equation, the constant σ can be scaled out, which will allow us to analytically obtain the oscillating-tail formula for all values of σ . This contrasts the original equation (1) where σ cannot be scaled out. The appropriate scaling to Eq. (9) is

$$\kappa = \frac{1}{\sigma}\hat{\kappa}, \quad \lambda = \frac{1}{\sigma}\hat{\lambda}, \quad U(\kappa) = U\left(\frac{1}{\sigma}\hat{\kappa}\right) \equiv \widehat{U}(\hat{\kappa}). \tag{10}$$

Under this scaling, the outer equation reduces to

$$(1 - \hat{\epsilon}\hat{\kappa}^2)\widehat{U} - \int_0^{\hat{\kappa}} \widehat{U}(\hat{\lambda})\widehat{U}(\hat{\kappa} - \hat{\lambda})d\hat{\lambda} = 1, \tag{11}$$

where $\hat{\epsilon} \equiv \epsilon/\sigma^2$. This equation can be solved by power series,

$$\widehat{U}(\hat{\kappa}) = \sum_{m=1}^{\infty} \hat{a}_m(\sqrt{\hat{\epsilon}}\hat{\kappa})^{m-1}, \tag{12}$$

where the coefficients \hat{a}_m satisfy the following recurrence relation:

$$\hat{a}_m - \hat{a}_{m-2} - \frac{1}{\sqrt{\hat{\epsilon}}} \sum_{r=1}^{m-1} \frac{(r-1)!(m-r-1)!}{(m-1)!} \hat{a}_r \hat{a}_{m-r} = 0, \quad m \geq 3, \tag{13}$$

and

$$\hat{a}_1 = 1, \quad \hat{a}_2 = \hat{\epsilon}^{-1/2}, \tag{14}$$

to be consistent with expansion (4). At large m , the coefficients \hat{a}_m have the following asymptotics:

$$\hat{a}_m \sim D(\hat{\epsilon}) m^{1/\sqrt{\hat{\epsilon}}}, \quad m \gg 1, \tag{15}$$

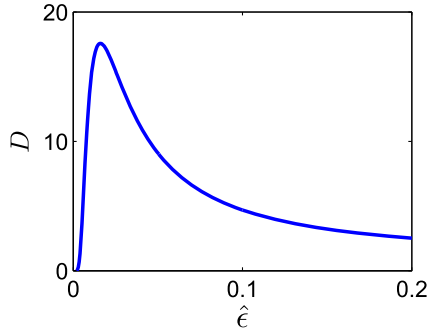


Figure 2. Graph of function $D(\hat{\epsilon})$ for the recurrence problem (13)–(15).

where the positive constant $D(\hat{\epsilon})$ depends on $\hat{\epsilon}$ but is independent of m . This asymptotics will also be confirmed in the next section (by analyzing the behavior of the inner equation, see Eq. (35)). As we will also show in the next section, this \hat{a}_m asymptotics indicates that the solution to the outer equation (9) features a pole at $\kappa = \kappa_0$ with order $1/\sqrt{\hat{\epsilon}} + 1$ (see Eq. (31)). This order of the pole may also be obtained directly from the outer equation through dominant balance. For arbitrary $\hat{\epsilon}$, this order is not an integer in general. This contrasts all previous cases of exponential asymptotics calculations in the wave number domain, where the pole in the solution to the outer equation always has an integer order [14, 15, 22, 24, 25, 27].

Numerically, we have obtained the graph of function $D(\hat{\epsilon})$, which is shown in Fig. 2. Notice that $D(\hat{\epsilon})$ has a nonsimple functional form, even for small $\hat{\epsilon}$ such as $\hat{\epsilon} \sim 0.02$. We have also found that

$$D(1) \approx 0.9432, \quad D(\infty) = 1/2. \quad (16)$$

These D values will show that our exponential asymptotics results can recover those in [27] with weaker nonlinearity or no nonlinearity as special cases. More will be said on this at the end of this section.

In view of the scaling introduced in (10), the solution to the unscaled outer equation (9) is

$$U(\kappa) = \sum_{m=1}^{\infty} a_m (\sqrt{\epsilon} \kappa)^{m-1}, \quad (17)$$

where

$$a_m = \hat{a}_m \sim D(\hat{\epsilon}) m^{1/\sqrt{\hat{\epsilon}}}, \quad m \gg 1. \quad (18)$$

2.2. The inner equation

Near the pole ($\kappa \sim \kappa_0$), the outer equation (9) is invalid, and a different approximation to the original equation (8) is needed. To this end, we introduce the inner variable $\xi = (\kappa - \kappa_0)/\sqrt{\epsilon}$. When $\xi = O(1)$, dominant contributions to the integral of Eq. (8) come from the $\lambda \sim 0$ and $\lambda \sim \kappa$ regions. Utilizing the asymptotics (7) and the ϵ -scaling of $U(\xi)$ to be found in Eq. (28), Eq. (8) then reduces to

$$\sqrt{\epsilon} \xi U(\xi) + \frac{1}{2} \sigma \int_{-\infty}^{\infty} e^{\pi\lambda/2} \operatorname{sech} \frac{\pi\lambda}{2} U(\xi - \lambda) d\lambda = 0. \tag{19}$$

This inner equation is almost the same as that derived in [27], except for the $\sqrt{\epsilon}$ factor that proves to be important. This $\sqrt{\epsilon}$ factor is a consequence of nonlinearity dominating dispersion, and it makes the inner solution very different from that in [27] as we will see below.

Defining the same scaled parameter $\hat{\epsilon} = \epsilon/\sigma^2$, this inner equation becomes

$$\sqrt{\hat{\epsilon}} \xi U(\xi) + \frac{1}{2} \int_{-\infty}^{\infty} e^{\pi\lambda/2} \operatorname{sech} \frac{\pi\lambda}{2} U(\xi - \lambda) d\lambda = 0. \tag{20}$$

Since the integral is of convolution type, its solution can be postulated as a half line Fourier transform [27]

$$U(\xi) = \int_0^{\pm\infty} e^{-is\xi} \phi(s) ds, \tag{21}$$

where the \pm sign in the upper limit is chosen for ξ in the lower and upper half of the ξ plane, respectively. Inserting this transform into the integral equation (20), exchanging the order of integration and utilizing the formula

$$\int_{-\infty}^{\infty} \frac{1}{2} \operatorname{sech} \frac{\pi\lambda}{2} e^{ik\lambda} d\lambda = \operatorname{sech} k, \tag{22}$$

this integral equation becomes

$$\int_0^{\pm\infty} e^{-is\xi} \left[\sqrt{\hat{\epsilon}} \frac{d\phi}{ds} - \frac{\phi}{\sinh s} \right] ds = 0; \tag{23}$$

thus, the function $\phi(s)$ satisfies the differential equation

$$\sqrt{\hat{\epsilon}} \frac{d\phi}{ds} - \frac{\phi}{\sinh s} = 0. \tag{24}$$

This differential equation may be solved exactly as

$$\phi(s) = C \left[2 \tanh \frac{s}{2} \right]^{1/\sqrt{\hat{\epsilon}}}, \tag{25}$$

where C is a constant to be found by matching with the outer solution. Substituting Eqs. (21) and (25) into (19), exchanging the order of integration and utilizing the formula (22) again, we find an alternative expression for the solution $U(\xi)$ that has a wider domain of analyticity,

$$U(\xi) = \frac{-i}{\sqrt{\hat{\epsilon}} \xi} \int_0^{\pm\infty} e^{-is\xi} \frac{\phi(s)}{\sinh s} ds, \tag{26}$$

or equivalently,

$$U(\xi) = \frac{-iC}{\sqrt{\hat{\epsilon}} \xi} \int_0^{\pm\infty} e^{-is\xi} \frac{[2 \tanh \frac{s}{2}]^{1/\sqrt{\hat{\epsilon}}-1}}{\cosh^2 \frac{s}{2}} ds. \tag{27}$$

Below, we will only take the plus sign in the upper limit of the integral, which yields a solution for $U(\xi)$ valid in the lower half of the ξ plane and analytically extendable to the strip $0 < \text{Im}(\xi) < 1$ in the upper half plane. This solution will be suitable for calculating the physical solution $u(x)$ that decays upstream ($x \rightarrow -\infty$) and has an oscillating tail downstream.

The asymptotics of this solution for $U(\xi)$ can be readily obtained. When $\xi \rightarrow 0$, the integral in the solution expression (27) approaches a constant and gives us the asymptotics

$$U(\xi) \rightarrow -iC \frac{2^{1/\sqrt{\hat{\epsilon}}}}{\xi}, \quad \xi \rightarrow 0, \tag{28}$$

which has a simple pole of residue $-i2^{1/\sqrt{\hat{\epsilon}}}C$ at $\xi = 0$. When $\xi \rightarrow -\infty$, by changing the path of integration in the solution expression (21) to the upper imaginary s -axis (which is the path of steepest descent), we find that the dominant contribution to the integral comes from the $s \approx 0$ region, and thus

$$U(\xi) \rightarrow \frac{\hat{C}}{(-\xi)^{1/\sqrt{\hat{\epsilon}}+1}}, \quad \xi \rightarrow -\infty, \tag{29}$$

where

$$\hat{C} \equiv i^{1/\sqrt{\hat{\epsilon}}+1} \Gamma\left(\frac{1}{\sqrt{\hat{\epsilon}}} + 1\right) C. \tag{30}$$

This large- ξ asymptotics of the inner solution needs to match the asymptotics of the outer solution as $\kappa \rightarrow \kappa_0$. In terms of the outer variable κ , the asymptotics (29) reads

$$U(\kappa) \sim \hat{C} \epsilon^{1/\sqrt{\hat{\epsilon}}+1} \frac{1}{\left(1 - \frac{\kappa}{\kappa_0}\right)^{1/\sqrt{\hat{\epsilon}}+1}}, \quad \kappa \sim \kappa_0, \tag{31}$$

which shows that the solution to the outer equation (9) has a pole at $\kappa = \kappa_0$ with order $1/\sqrt{\hat{\epsilon}} + 1$. To connect the above behavior with the power series solution (17) of the outer equation, we Taylor-expand the above function as

$$U(\kappa) \sim \frac{\widehat{C}\epsilon^{1/\sqrt{\hat{\epsilon}}+1}}{\left(\frac{1}{\sqrt{\hat{\epsilon}}}\right)!} \sum_{m=1}^{\infty} \frac{\left(\frac{1}{\sqrt{\hat{\epsilon}}} + m - 1\right)!}{(m - 1)!} (\sqrt{\epsilon} \kappa)^{m-1}. \tag{32}$$

Comparing this with the Taylor series (17) of the outer solution, we see that

$$a_m \sim \frac{\widehat{C}\epsilon^{1/\sqrt{\hat{\epsilon}}+1}}{\Gamma\left(\frac{1}{\sqrt{\hat{\epsilon}}} + 1\right)} \frac{\Gamma\left(\frac{1}{\sqrt{\hat{\epsilon}}} + m\right)}{\Gamma(m)}, \quad m \gg 1. \tag{33}$$

Using the large- x asymptotics of the $\Gamma(x)$ function,

$$\Gamma(x) \sim \sqrt{2\pi} x^{x-\frac{1}{2}} e^{-x}, \quad x \gg 1, \tag{34}$$

we find that

$$a_m \sim \frac{\widehat{C}\epsilon^{1/\sqrt{\hat{\epsilon}}+1}}{\Gamma\left(\frac{1}{\sqrt{\hat{\epsilon}}} + 1\right)} m^{1/\sqrt{\hat{\epsilon}}}, \quad m \gg 1. \tag{35}$$

Comparing this asymptotics with (18) and utilizing the \widehat{C} expression (30), we then find that

$$C = \frac{D(\hat{\epsilon})}{(i\epsilon)^{1/\sqrt{\hat{\epsilon}}+1}}. \tag{36}$$

Inserting this C formula into (28), we obtain the behavior of the solution $U(\xi)$ near the pole as

$$U(\xi) \rightarrow -\frac{D(\hat{\epsilon})}{\epsilon} \left(\frac{2}{i\epsilon}\right)^{1/\sqrt{\hat{\epsilon}}} \frac{1}{\xi}, \quad \xi \rightarrow 0. \tag{37}$$

Substituting this into (6), we then get the pole behavior in the original Fourier transform $\hat{u}(k)$ as

$$\hat{u}(k) \sim -\frac{D(\hat{\epsilon})}{\epsilon} \left(\frac{2}{i\epsilon}\right)^{1/\sqrt{\hat{\epsilon}}} \frac{e^{-\frac{\pi}{2\epsilon}}}{k - \frac{1}{\epsilon}}, \quad k \rightarrow \frac{1}{\epsilon}. \tag{38}$$

Since $u(x)$ is real, its Fourier transform $\hat{u}(k)$ admits the symmetry

$$\hat{u}(-k) = \hat{u}^*(k) \tag{39}$$

for real k . Using this symmetry, we can easily derive the behavior of the solution $\hat{u}(k)$ at the other pole $k = -1/\epsilon$.

2.3. Oscillating tails

Finally, we take the inverse Fourier transform

$$u(x) = \int_{-\infty}^{\infty} \hat{u}(k)e^{ikx} dk \tag{40}$$

to recover the physical solution. To make $u(x)$ decay upstream, we choose the integration path to pass below the two poles at $k = \pm 1/\epsilon$. Then, using the residue theorem, we find that downstream,

$$u(x) \sim -\frac{2\pi i D(\hat{\epsilon})}{\epsilon} \left(\frac{2}{i\epsilon}\right)^{\frac{1}{\sqrt{\epsilon}}} e^{-\frac{\pi}{2\epsilon} + i\frac{x}{\epsilon}} + c.c., \quad x \gg 1, \tag{41}$$

which simplifies to

$$u(x) \rightarrow R \sin \frac{1}{\epsilon}(x - \theta), \quad x \rightarrow \infty, \tag{42}$$

where the tail amplitude R and phase θ are given by

$$R = \frac{4\pi D\left(\frac{\epsilon}{\sigma^2}\right)}{\epsilon} e^{-\frac{\pi}{2\epsilon} + \frac{\sigma}{\sqrt{\epsilon}} \ln\left(\frac{2}{\epsilon}\right)}, \quad \theta = \frac{\pi\sigma\sqrt{\epsilon}}{2}. \tag{43}$$

The R formula shows that the tail amplitude is indeed exponentially small, which is expected. However, an unexpected feature of this R formula is that, in addition to the usual $\exp(-\frac{\pi}{2\epsilon})$ factor, it also contains a factor $\exp(\frac{\sigma}{\sqrt{\epsilon}} \ln(\frac{2}{\epsilon}))$, which has not been seen before. This latter factor is induced by the nonlinearity dominating dispersion, and is one of the main new aspects of this exponential asymptotics analysis.

We have compared these formulas with numerics for a fixed value of $\sigma = 1/2$ and various values of ϵ , and the comparison results are presented in Fig. 3. One can see that the analytical and numerical results approach each other as ϵ decreases, confirming the asymptotic nature of our formulas.

In the analysis above, the nonlinear coefficient σ was treated as an arbitrary but $O(1)$ parameter. Interestingly, our results are also valid when $\sigma = \sqrt{\epsilon}$ and 0. The former case has a weaker nonlinearity and has been treated before [27]. In this case, our formulas (42) and (43) reduce to

$$u(x) \rightarrow -\frac{8\pi D(1)}{\epsilon^2} e^{-\frac{\pi}{2\epsilon}} \cos \frac{x}{\epsilon}, \quad x \rightarrow \infty, \tag{44}$$

where $D(1)$ is given in Eq. (16). This formula exactly matches that in [27]. In the latter case, $\sigma = 0$, there is no nonlinearity. Utilizing the value $D(\infty) = 1/2$ in (16), our formulas (42) and (43) reduce to

$$u(x) \rightarrow \frac{2\pi}{\epsilon} e^{-\frac{\pi}{2\epsilon}} \sin \frac{x}{\epsilon}, \quad x \rightarrow \infty, \tag{45}$$

which again matches the linear tail in [27] exactly.

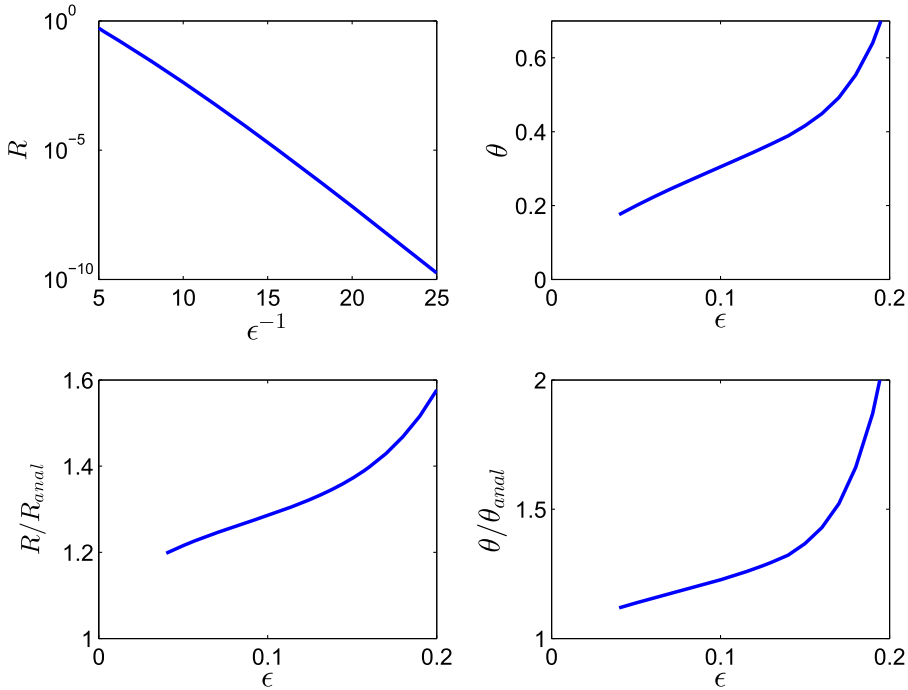


Figure 3. Comparison of the amplitude and phase of the oscillating tail between numerics and the analytical formulas (43) for $\sigma = 0.5$ and various ϵ in the problem (1)–(2). Upper left: numerical tail versus $1/\epsilon$. Upper right: numerical phase versus ϵ . Lower left: the ratio between numerical tail size and the analytical formula (43) versus ϵ . Lower right: the ratio between numerical phase and analytical formula (43) versus ϵ .

3. Oscillatory tails in a steady-state forced NLS equation

In our second example, we consider the steady-state NLS equation with a complex forcing:

$$u + \epsilon^2 u_{xx} - \epsilon \sigma |u|^2 u = \operatorname{sech} \left(x - i \frac{\alpha}{2} \right), \tag{46}$$

subject to the boundary condition

$$u(x) \rightarrow 0, \quad x \rightarrow -\infty. \tag{47}$$

Here, $0 < \epsilon \ll 1$, σ is a positive free parameter, and $0 < \alpha < \pi$ is another free parameter. This choice of forcing is motivated by the so-called coupled mode equations, which are the appropriate envelope equations near the opening of a bandgap in periodic media and admit soliton solutions with the same complex “sech” form [6]. Equation (46) admits solutions that decay upstream and exhibit oscillatory tails downstream ($x \rightarrow \infty$). An example of such a solution is displayed in Fig. 4. Again, the amplitudes

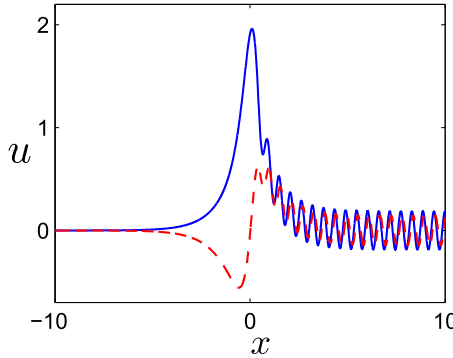


Figure 4. A solution $u(x)$ to Eqs. (46) and (47) with $\sigma = 0.7$, $\alpha = \pi/2$, and $\epsilon = 0.09$. Solid blue: $\text{Re}(u)$; dashed red: $\text{Im}(u)$.

of these oscillatory tails are exponentially small in ϵ , and we will develop exponential asymptotics below to calculate them.

In this example, the Fourier transform of the forcing decays faster for $k \rightarrow -\infty$ than for $k \rightarrow \infty$. As a result, in the perturbation expansion in the wave number domain, the dominant behavior for $k \rightarrow -\infty$ is dictated by higher order terms that decay more slowly (see Eq. (49)). Because of this, approximating the convolution integrals in the wave number domain resulting from the nonlinear term in Eq. (46) becomes more complicated than before, and reductions to a single outer or inner equation are no longer possible.

A straightforward perturbation expansion of the solution in ϵ gives

$$u(x) \sim u_0 + \epsilon \sigma |u_0|^2 u_0 - \epsilon^2 u_{0xx} + 3\epsilon^2 \sigma^2 |u_0|^4 u_0 + \dots, \tag{48}$$

where $u_0(x) = \text{sech}(x - i\frac{\alpha}{2})$. The Fourier transform of this perturbation solution is

$$\begin{aligned} \widehat{u}(k) \sim \widehat{u}_0(k) & \left[1 + \epsilon \sigma \csc(\alpha) k + \epsilon^2 k^2 + \frac{3}{2} \epsilon^2 \sigma^2 \csc^2(\alpha) k^2 + \dots \right] \\ & + \epsilon \sigma \widehat{v}_0(k) \csc^2 \alpha [1 + 3\epsilon \sigma \csc(\alpha) k + \dots], \end{aligned} \tag{49}$$

where

$$\widehat{u}_0(k) = \frac{1}{2} \text{sech}\left(\frac{\pi}{2} k\right) e^{k\alpha/2} \tag{50}$$

is the Fourier transform of $u_0(x)$, and $\widehat{v}_0(k) = \widehat{u}_0^*(-k)$ is the Fourier transform of $v_0(x) \equiv u_0^*(x)$.

It is important to notice that $\widehat{u}_0(k)$ has different decay rates along the positive and negative k directions,

$$\widehat{u}_0(k) \rightarrow \begin{cases} e^{-(\pi-\alpha)k/2}, & k \rightarrow \infty, \\ e^{(\pi+\alpha)k/2}, & k \rightarrow -\infty; \end{cases} \quad (51)$$

i.e., it decays slower along the positive k direction. Since $\widehat{v}_0(k) = \widehat{u}_0^*(-k)$, $\widehat{v}_0(k)$ decays faster along the positive k direction. As a consequence, the Fourier transform $\widehat{u}_0(k)$ has differing asymptotic behaviors as $k \rightarrow \pm\infty$.

- (1) For $k \gg 1$, since $\widehat{v}_0(k)$ decays more rapidly than $\widehat{u}_0(k)$, the $\epsilon\widehat{v}_0(k)$ terms in (49) are subdominant.
- (2) For $k \ll -1$, however, $\widehat{v}_0(k)$ decays slower than $\widehat{u}_0(k)$. Thus, the $\epsilon\widehat{v}_0(k)$ terms actually become dominant.

These disparate asymptotic behaviors of $\widehat{u}(k)$ in the positive and negative k directions will be important when computing convolution integrals in the wave number domain.

The perturbation series (49) becomes disordered for $\kappa \equiv \epsilon k = O(1)$. Upon taking the Fourier transform of the original equation (46), using $v \equiv u^*$ and the κ scaling, we get the following set of coupled integral equations:

$$\widehat{u} - \kappa^2 \widehat{u} - \frac{\sigma}{\epsilon} \int_{-\infty}^{\infty} \int_{-\infty}^{\infty} \widehat{u}(\kappa - \lambda) \widehat{u}(\lambda - r) \widehat{v}(r) dr d\lambda = \widehat{u}_0, \quad (52a)$$

$$\widehat{v} - \kappa^2 \widehat{v} - \frac{\sigma}{\epsilon} \int_{-\infty}^{\infty} \int_{-\infty}^{\infty} \widehat{v}(\kappa - \lambda) \widehat{v}(\lambda - r) \widehat{u}(r) dr d\lambda = \widehat{v}_0. \quad (52b)$$

Here, the solution $\widehat{u}(k)$ does not exhibit the same symmetry (39) as the previous example because $u(x)$ is complex now. As a consequence, the pole behaviors at $\kappa = \pm 1$ will be different and coupled.

3.1. Outer equation

For $\kappa > 0$, due to the subdominant nature of the $\epsilon\widehat{v}_0(k)$ terms in (49), we assume the leading-order solution of $\widehat{u}(k)$ in the form

$$\widehat{u}(k) \sim U(\kappa) \widehat{u}_0(k). \quad (53)$$

For the solution $\widehat{v}(k) = \widehat{u}(-k)^*$, however, its tail contains both rapidly decaying terms starting at $O(1)$ and slowly decaying terms starting at $O(\epsilon)$. Thus, $\widehat{v}(k)$ for $\kappa > 0$ is assumed to take the form

$$\widehat{v}(k) = U^*(-\kappa) \widehat{v}_0(k) + \epsilon V(\kappa) \widehat{u}_0(k). \quad (54)$$

Since $\widehat{v}_0(k)$ decays much more rapidly than $\widehat{u}_0(k)$ as k grows large, the proper approximation is

$$\widehat{v}(k) \sim \begin{cases} \widehat{v}_0(k)U^*(-\kappa), & 0 < \kappa \ll 1, \\ \epsilon\widehat{u}_0(k)V(\kappa), & \kappa = O(1). \end{cases} \tag{55}$$

Our idea for simplifying the double convolutions in Eqs. (52) can be understood from treating a single convolution. Specifically, consider the single convolution $\int_{-\infty}^{\infty} \widehat{u}(\kappa - \lambda)\widehat{v}(\lambda)d\lambda$, which is

$$\int_{-\infty}^{\infty} U(\kappa - \lambda)\widehat{u}_0\left(\frac{\kappa - \lambda}{\epsilon}\right) \left[U^*(-\lambda)\widehat{v}_0\left(\frac{\lambda}{\epsilon}\right) + \epsilon V(\lambda)\widehat{u}_0\left(\frac{\lambda}{\epsilon}\right) \right] d\lambda.$$

Contributions to this integral can be broken into four intervals,

$$(-\infty, -\delta), \quad (-\delta, \delta), \quad (\delta, \kappa), \quad (\kappa, \infty),$$

where δ is an introduced parameter to split the intervals. We choose $\epsilon \ll \delta \ll 1$, which allows δ to be large enough for the exponential decay to dominate the solution behavior, but small enough to avoid encroachment on the interval $0 < \lambda < \kappa$. Next, we calculate these four contributions when κ is away from any poles.

The contribution from the second interval $(-\delta, \delta)$ is

$$\begin{aligned} I_2 &= \int_{-\delta}^{\delta} \widehat{u}(\kappa - \lambda)\widehat{v}(\lambda)d\lambda \\ &\approx \int_{-\delta}^{\delta} (U(\kappa - \lambda)e^{-(\pi-\alpha)(\kappa-\lambda)/2\epsilon}) U^*(-\lambda)\widehat{v}_0(\lambda/\epsilon)d\lambda \\ &\approx \epsilon U(\kappa)U^*(0)e^{-(\pi-\alpha)\kappa/2\epsilon} \int_{-\delta/\epsilon}^{\delta/\epsilon} e^{(\pi-\alpha)r/2}\widehat{v}_0(r)dr \\ &\approx \epsilon U(\kappa)(1)e^{-(\pi-\alpha)\kappa/2\epsilon} \int_{-\infty}^{\infty} \frac{1}{2}\operatorname{sech}\left(\frac{\pi r}{2}\right) e^{(\frac{\pi}{2}-\alpha)r} dr \\ &= \epsilon e^{-(\pi-\alpha)\kappa/2\epsilon} U(\kappa) \csc(\alpha). \end{aligned}$$

In the third interval (δ, κ) , $\widehat{v}(\lambda)$ is approximated by its slowly decaying tail terms at order ϵ , see Eq. (55). Thus,

$$\begin{aligned} I_3 &= \int_{\delta}^{\kappa} \widehat{u}(\kappa - \lambda)\widehat{v}(\lambda)d\lambda \\ &\approx \int_{\delta}^{\kappa} (e^{-(\pi-\alpha)(\kappa-\lambda)/2\epsilon} U(\kappa - \lambda)) (\epsilon e^{-(\pi-\alpha)\lambda/2\epsilon} V(\lambda)) d\lambda \\ &\approx \epsilon e^{-(\pi-\alpha)\kappa/2\epsilon} \int_0^{\kappa} U(\kappa - \lambda)V(\lambda)d\lambda. \end{aligned}$$

The remaining two regions make smaller contributions and may be ignored, since

$$I_1 = \int_{-\infty}^{-\delta} \widehat{u}(\kappa - \lambda)\widehat{v}(\lambda)d\lambda \sim O\left(\epsilon e^{-(\pi-\alpha)\delta/\epsilon} e^{-(\pi-\alpha)\kappa/2\epsilon}\right),$$

$$I_4 = \int_{\kappa}^{\infty} \widehat{u}(\kappa - \lambda)\widehat{v}(\lambda)d\lambda \sim O\left(\epsilon^2 e^{-(\pi-\alpha)\kappa/2\epsilon}\right).$$

Collecting all these contributions, we get a final approximation for the single convolution integral as

$$\int_{-\infty}^{\infty} \widehat{u}(\kappa - \lambda)\widehat{v}(\lambda)d\lambda \approx \epsilon e^{-(\pi-\alpha)\kappa/2\epsilon} \left(\csc(\alpha)U(\kappa) + \int_0^{\kappa} U(\kappa - \lambda)V(\lambda)d\lambda \right).$$

Using the above procedure as a guide, approximating the double convolution integrals in (52) gives the following outer equations for $\kappa > 0$ and away from any poles,

$$U - \kappa^2 U - \sigma \int_0^{\kappa} \int_0^{\lambda} U(\kappa - \lambda)U(\lambda - r)V(r)drd\lambda - \sigma \csc(\alpha) \int_0^{\kappa} U(\kappa - \lambda)U(\lambda)d\lambda = 1, \tag{56a}$$

$$V - \kappa^2 V - \sigma \int_0^{\kappa} \int_0^{\lambda} V(\kappa - \lambda)V(\lambda - r)U(r)drd\lambda - 2\sigma \csc(\alpha) \int_0^{\kappa} V(\kappa - \lambda)U(\lambda)d\lambda - \sigma \csc^2(\alpha)U = 0. \tag{56b}$$

To be consistent with (49), the initial conditions to these outer equations are

$$U(0) = 1, \quad V(0) = \sigma \csc^2(\alpha). \tag{57}$$

Using dominant balance, we find that near the pole singularity ($\kappa \rightarrow 1$), the leading order behaviors of $U(\kappa)$ and $V(\kappa)$ are

$$U(\kappa) \sim \widehat{A}(1 - \kappa)^{-(p+1)}, \tag{58a}$$

$$V(\kappa) \sim \widehat{B}(1 - \kappa)^{-(p+2)}, \tag{58b}$$

where constants p , \widehat{A} , and \widehat{B} satisfy the system of equations

$$0 = 2\widehat{A} - \sigma \frac{\widehat{B}}{p(p+1)} - 2\sigma \csc(\alpha) \frac{\widehat{A}}{p}, \tag{59a}$$

$$0 = 2\widehat{B} - 2\sigma \csc(\alpha) \frac{\widehat{B}}{(p+1)} - \sigma \csc^2(\alpha)\widehat{A}. \tag{59b}$$

For nontrivial solutions to be possible, we find that

$$p = \frac{1}{2} \left(-1 + 2\sigma \csc(\alpha) + \sqrt{1 + \sigma^2 \csc^2(\alpha)} \right), \tag{60}$$

and \widehat{B} can be expressed in terms of \widehat{A} as

$$\widehat{B} = \frac{2}{\sigma} (p + 1) [p - \sigma \csc(\alpha)] \widehat{A}, \tag{61}$$

where \widehat{A} is a constant that can be determined by solving the coupled outer equations (56) numerically. For generic values of σ and α , p is not an integer. Thus, in this problem, the orders of the poles in the outer solution are again noninteger in general, which resembles the first example in the previous section but contrasts exponential asymptotics calculations done before in the wave number domain [14, 15, 22, 24, 25, 27].

3.2. Inner equation

Near the pole at $k_0 = 1/\epsilon$, we define the inner variable $\xi = (k - k_0)/\epsilon$, and propose the inner solutions in the form

$$\widehat{u}(\xi) = \epsilon^{-(p+1)} \widehat{u}_0(k) \phi(\xi), \tag{62a}$$

$$\widehat{v}(\xi) = \epsilon^{-(p+1)} \widehat{u}_0(k) \psi(\xi). \tag{62b}$$

The ϵ scaling here is deduced from the requirement that this inner solution at $|\xi| \gg 1$ should match the outer solution near the pole ($\kappa \sim 1$), with the latter provided by Eqs. (53), (54), and (58). In fact, this matching condition provides not only the correct ϵ scaling above, but also the large- ξ asymptotics of the inner solution, which coincides with the one obtained independently from the analysis of the inner equation below (see (70)).

For k values near the pole, the main contributions to the double convolutions in (52) come from the three regions: (i) $\lambda \approx r \approx 0$; (ii) $\lambda \approx 1, r \approx 0$; and (iii) $\lambda \approx r \approx 1$. In these regions, one of the three terms in the integrand is near the pole, and the other two terms are in the small wave number regimes. In this case, the full equations (52) reduce to the following coupled inner equations for $\phi(\xi)$ and $\psi(\xi)$:

$$2\xi\phi + \sigma \int_{-\infty}^{\infty} e^{\lambda(\pi-\alpha)/2} \left(2\widehat{u}_0\widehat{v}_0(\lambda)\phi(\xi - \lambda) + \widehat{u}_0^2(\lambda)\psi(\xi - \lambda) \right) d\lambda = 0, \tag{63a}$$

$$2\xi\psi + \sigma \int_{-\infty}^{\infty} e^{\lambda(\pi-\alpha)/2} \left(2\widehat{u}_0\widehat{v}_0(\lambda)\psi(\xi - \lambda) + \widehat{v}_0^2(\lambda)\phi(\xi - \lambda) \right) d\lambda = 0. \tag{63b}$$

These are solved by half-line Fourier transforms

$$\phi(\xi) = \int_0^{\infty} \widetilde{\phi}(s) e^{-is\xi} ds, \tag{64a}$$

$$\psi(\xi) = \int_0^\infty \tilde{\psi}(s)e^{-is\xi} ds, \tag{64b}$$

for ξ in the lower half plane. This transform converts the coupled integral equations (63) into coupled differential equations

$$0 = -2i \frac{d\tilde{\phi}}{ds} - \sigma 2\text{csch}(s)\text{csch}(s + i\alpha)\tilde{\phi} - \sigma \text{csch}^2(s)\tilde{\psi}, \tag{65a}$$

$$0 = -2i \frac{d\tilde{\psi}}{ds} - \sigma 2\text{csch}(s)\text{csch}(s + i\alpha)\tilde{\psi} - \sigma \text{csch}^2(s + i\alpha)\tilde{\phi}. \tag{65b}$$

To solve these homogeneous differential equations, initial conditions are needed. These initial conditions can be obtained from local analysis of these equations in the limit of $s \rightarrow 0$. Using dominant balance, we find that

$$\tilde{\phi}(s) \sim As^p, \quad s \rightarrow 0, \tag{66a}$$

$$\tilde{\psi}(s) \sim Bs^{p+1}, \quad s \rightarrow 0, \tag{66b}$$

where p is the same constant found in (60), and the parameters A and B are related by

$$B = -\frac{2i}{\sigma}[p - \sigma \csc(\alpha)]A. \tag{67}$$

These parameter values will be determined by matching the inner solutions to the outer ones (see Eq. (71)).

The set of differential equations (65) do not seem to admit a closed-form analytical solution; so, instead, we settle for a numerical solution. Once $\tilde{\phi}(s)$ and $\tilde{\psi}(s)$ have been computed, we insert the transform (64) back into the inner equations (63). Then, upon exchange of order of integration and simple manipulation, the solution to the inner equations can be expressed alternatively as

$$\phi(\xi) = \frac{\sigma}{2\xi} \int_0^\infty (2\text{csch}(s)\text{csch}(s + i\alpha)\tilde{\phi}(s) + \text{csch}^2(s)\tilde{\psi}(s)) e^{-is\xi} ds, \tag{68a}$$

$$\psi(\xi) = \frac{\sigma}{2\xi} \int_0^\infty (2\text{csch}(s)\text{csch}(s + i\alpha)\tilde{\psi}(s) + \text{csch}^2(s + i\alpha)\tilde{\phi}(s)) e^{-is\xi} ds, \tag{68b}$$

which have a wider domain of analyticity in the ξ plane. These formulas show that $\phi(\xi)$ and $\psi(\xi)$ have a simple pole at $\xi = 0$, and their residues are

$$R_\phi = \frac{\sigma}{2} \int_0^\infty (2\text{csch}(s)\text{csch}(s + i\alpha)\tilde{\phi}(s) + \text{csch}^2(s)\tilde{\psi}(s)) ds, \tag{69a}$$

$$R_\psi = \frac{\sigma}{2} \int_0^\infty (2\text{csch}(s)\text{csch}(s + i\alpha)\tilde{\psi}(s) + \text{csch}^2(s + i\alpha)\tilde{\phi}(s)) ds. \tag{69b}$$

As $\xi \rightarrow \pm\infty$, the dominant contributions in the solution expressions (64) come from the $s \approx 0$ region. Inserting the $s \rightarrow 0$ asymptotics (66) of $\tilde{\phi}$ and $\tilde{\psi}$ into (64), large- ξ asymptotics of ϕ and ψ are found to be

$$\phi(\xi) \sim A \frac{\Gamma(p+1)}{(i\xi)^{p+1}}, \tag{70a}$$

$$\psi(\xi) \sim B \frac{\Gamma(p+2)}{(i\xi)^{p+2}}. \tag{70b}$$

This large- ξ asymptotics of the inner solution should match the $\kappa \rightarrow 1$ asymptotics (58) of the outer solution. This matching yields

$$A = \frac{(-i)^{p+1}}{\Gamma(p+1)} \widehat{A}, \tag{71a}$$

$$B = \frac{(-i)^{p+2}}{\Gamma(p+2)} \widehat{B}, \tag{71b}$$

which allows us to find the correct choice of parameter A in terms of the numerically computed \widehat{A} from the outer equation. After the value of A is obtained, the inner differential equations (65), subject to the initial conditions (66), can be uniquely solved. Then, the residues R_ϕ and R_ψ can be derived from (69).

3.3. Tail calculation

The formula for the oscillating tails comes from the poles of $\widehat{u}(k)$ at $k = \pm 1/\epsilon$. After the residues R_ϕ and R_ψ are obtained, the near-pole behaviors of $\phi(k)$ and $\psi(k)$ are

$$\phi(k) \sim \frac{R_\phi}{k - 1/\epsilon}, \quad k \sim 1/\epsilon, \tag{72a}$$

$$\psi(k) \sim \frac{R_\psi}{k - 1/\epsilon}, \quad k \sim 1/\epsilon. \tag{72b}$$

Substituting these into Eqs. (62) and utilizing the relation $\widehat{v}(k) = \widehat{u}(-k)^*$, we obtain the behavior of $\widehat{u}(k)$ near the two poles $k = \pm 1/\epsilon$ as

$$\widehat{u}(k) \sim \epsilon^{-(p+1)} \frac{R_\phi}{k - 1/\epsilon} e^{-(\pi-\alpha)/2\epsilon}, \quad k \rightarrow \frac{1}{\epsilon} \tag{73a}$$

$$\widehat{u}(k) \sim -\epsilon^{-(p+1)} \frac{R_\psi^*}{k + 1/\epsilon} e^{-(\pi-\alpha)/2\epsilon}, \quad k \rightarrow -\frac{1}{\epsilon}. \tag{73b}$$

Finally we perform the inverse Fourier transform to recover the physical solution $u(x)$. As before, we pick a contour of integration for the inverse Fourier transform that passes below the two poles. From the residue

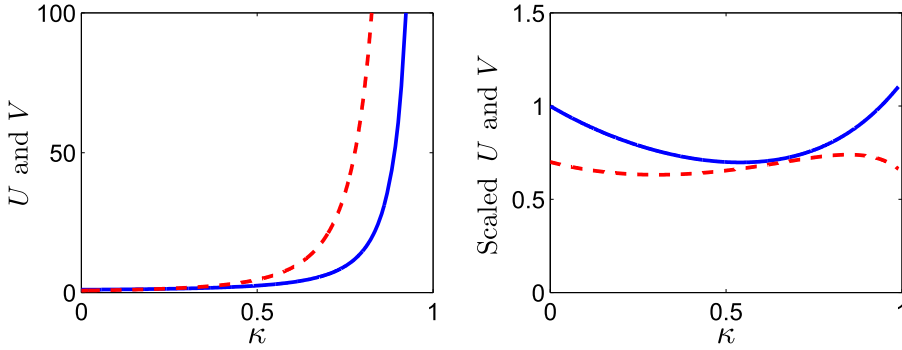


Figure 5. Solutions to the outer equations (56) and (57) for $\sigma = 0.7$ and $\alpha = \pi/2$. Left: the unscaled solutions $U(\kappa)$ (solid blue) and $V(\kappa)$ (dashed red). Right: the scaled solutions $U(\kappa)(1 - \kappa)^{p+1}$ (solid blue) and $V(\kappa)(1 - \kappa)^{p+2}$ (dashed red).

theorem, these two poles produce a tail of the form

$$u(x) \sim 2\pi i \epsilon^{-(p+1)} \left(R_\phi e^{ix/\epsilon} - R_\psi^* e^{-ix/\epsilon} \right) e^{-(\pi-\alpha)/2\epsilon}, \quad x \gg 1. \quad (74)$$

The amplitude of this tail is

$$R = 2\pi \left(|R_\phi| + |R_\psi| \right) \epsilon^{-(p+1)} e^{-(\pi-\alpha)/2\epsilon}, \quad (75)$$

which is exponentially small as anticipated.

We have compared these analytical oscillating tails with numerical results for a range of σ and α values and found good agreement. To illustrate, we take $\sigma = 0.7$ and $\alpha = \pi/2$. In this case, the solutions to the outer equations (56) and (57) are obtained numerically and displayed in Fig. 5. From the left panel, it is seen that these solutions develop singularities as $\kappa \rightarrow 1$. From the scaled solutions plotted in the right panel, we obtain the constants \widehat{A} and \widehat{B} as

$$\widehat{A} \approx 1.12, \quad \widehat{B} \approx 0.64.$$

These numbers satisfy the relation (61) as predicted. From these constants, the A and B values are derived from Eq. (71). Using these A, B values, the inner differential equations (65) and (66) are then numerically solved, which yields the residues

$$R_\phi \approx 1.00i, \quad R_\psi = -0.32,$$

and the analytical tail formulas (74) and (75) are thus fully prescribed.

We now compare these analytical tail formulas with numerical results. For this purpose, the wave tails are numerically computed for various values of ϵ , and the tail amplitude (defined as the maximum of the absolute value of

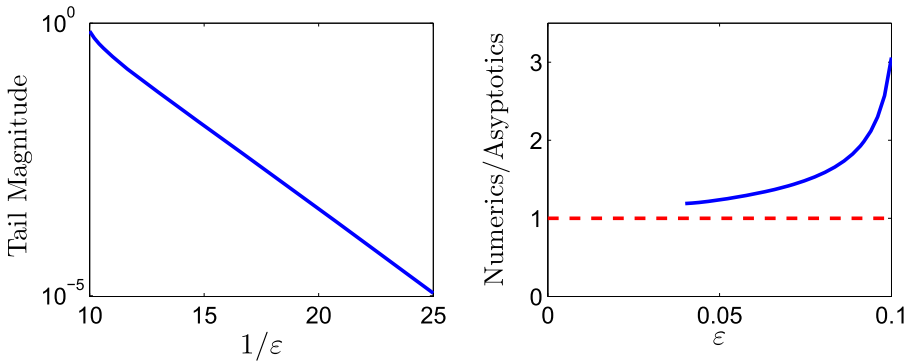


Figure 6. Comparison of the amplitude of the oscillating tail between numerics and the analytical formula (75) for $\sigma = 0.7$ and $\alpha = \pi/2$ and various ϵ in the problem (46)–(47). Left: the numerical tail size versus $1/\epsilon$. Right: the ratio between the numerical tail size and the analytical formula (75) versus ϵ . This ratio converges to 1 (dotted red) as $\epsilon \rightarrow 0$.

the oscillating tail) is plotted against ϵ in the left panel of Fig. 6. In the right panel, the ratio of the numerically computed tail amplitude and the asymptotic prediction (75) is plotted. It is seen that this ratio approaches 1 as $\epsilon \rightarrow 0$, which confirms the asymptotic accuracy of our analytical formulas.

4. Conclusion

We have presented exponential asymptotics techniques for computing short-scale oscillatory wave tails in two simple forced nonlinear wave problems. Our motivation for analyzing these model problems was to pave the way for understanding the bifurcation of gap solitons near the opening of a bandgap in periodic media, as the approach we successfully applied to gap solitons near edges of finite bandgaps in earlier work [22, 24, 25] encounters serious difficulties in this setting. Near the opening of a bandgap, two new obstacles arise: (i) the location of the poles in the wave number domain happens to be on a longer wave number scale than the nonlinear effects; (ii) the Fourier transform of the envelope solution features different decay rates in the positive and negative wave number directions, which causes the poles to be coupled and their residue calculation much more involved.

The examples discussed here were selected with the express purpose of addressing these two issues. Specifically, the first issue was tackled by considering a steady-state KdV equation with “sech” forcing, where nonlinearity is taken to be stronger than dispersion. In this model, the poles also appear on a longer wave number scale. As a consequence,

both the inner and outer reduced equations are ϵ -dependent, and the induced exponentially small tail has a rather intricate dependence on ϵ , as indicated by Eqs. (42) and (43). These asymptotic results are supported by numerical computations and also reduce to the already known tail expressions in the linear limit and in the case when nonlinearity balances dispersion [27].

The second issue was dealt with by considering a steady-state NLS equation with a complex “sech” forcing, whose Fourier transform decays faster for $k \rightarrow -\infty$ than $k \rightarrow \infty$. This asymmetry affects the analysis in the wave number domain in a highly nontrivial way, necessitating the solution of two coupled equations in the outer and inner regions in order to finally compute the pole residues and thereby the generated tails.

The exponential asymptotics techniques discussed here for simple model problems have laid the groundwork for analyzing the bifurcation of gap solitons near the opening of a bandgap in periodic media. As a specific example, consider the NLS equation with a weak spatially periodic potential. The linear spectrum comprises a countable infinity of bandgaps that emanate from specific frequencies when the potential strength tends to zero. Near the opening of each bandgap, a standard multiple-scale bifurcation theory shows that weakly nonlinear solutions are in the form of modulated wave packets whose envelope is governed by the so-called coupled-mode equations. These envelope equations admit envelope-soliton solutions that are translation-invariant, suggesting the existence of gap solitons irrespective of the position of the envelope relative to the periodic carrier. This, of course, is not true owing to the appearance of growing tails of exponentially small amplitude, necessitating the use of exponential asymptotics. The soliton solutions of the coupled-mode equations have the same complex “sech” form as the forcing of the NLS equation (46) treated in Section 3, where the Fourier transform of the solutions exhibits different decay rates along the positive and negative wave number directions. Accordingly, the exponential asymptotics procedure for computing these tails is expected to follow along similar lines as this model problem, taking also into account the modifications discussed in Section 2 due to the fact that nonlinearity also dominates dispersion in this setting. Details of the analysis of gap solitons near a stop-band opening will be reported elsewhere.

Acknowledgments

This material is based upon work supported by the Air Force Office of Scientific Research under award number FA9550-12-1-0244, and the National Science Foundation under award numbers DMS-1311730 and DMS-1616122.

References

1. D. J. BENNEY, A general theory for interactions between short and long waves, *Stud. Appl. Math.* 56:81–94 (1977).
2. D. J. BENNEY and A. C. NEWELL, Nonlinear wave envelopes, *J. Math. Phys.* 46:133–139 (1967).
3. D. J. BENNEY and G. J. ROSKES, Wave instabilities, *Stud. Appl. Math.* 48:377–385 (1969).
4. A. DAVEY and K. STEWARTSON, On three-dimensional packets of surface waves, *Proc. R. Soc. Lond. A* 338:101–110 (1974).
5. M. J. ABLOWITZ and H. SEGUR, *Solitons and the Inverse Scattering Transform*, SIAM, Philadelphia, 1981.
6. Y. KIVSHAR and G. AGRAWAL, *Optical Solitons: From Fibers to Photonic Crystals*, Academic Press, London, 2003.
7. J. YANG, *Nonlinear Waves in Integrable and Nonintegrable Systems*, SIAM, Philadelphia, 2010.
8. F. DALFOVO, S. GIORGINI, L. PITAEVSKII, and S. STRINGARI, Theory of Bose–Einstein condensation in trapped gases, *Rev. Mod. Phys.* 71:463–512 (1999).
9. Y. POMEAU, A. RAMANI, and B. GRAMMATICOS, Structural stability of the Korteweg–de Vries solitons under a singular perturbation, *Physica D* 31:127–134 (1988).
10. J. P. BOYD, Weakly non-local solitons for capillary-gravity waves: Fifth-degree Korteweg–de Vries equation, *Physica D* 48:129–146 (1991).
11. R. GRIMSHAW and N. JOSHI, Weakly nonlocal solitary waves in a singularly perturbed Korteweg–de Vries equation, *SIAM J. Appl. Math.* 55:124–135 (1995).
12. P. K. A. WAI, H. H. CHEN, and Y. C. LEE, Radiations by solitons at the zero-group-dispersion wavelength of single-mode optical fibers, *Phys. Rev. A* 41:426–439 (1990).
13. R. GRIMSHAW, Weakly nonlocal solitary waves in a singularly perturbed nonlinear Schrödinger equation, *Stud. Appl. Math.* 94:257–270 (1995).
14. D. C. CALVO and T. R. AKYLAS, On the formation of bound states by interacting nonlocal solitary waves, *Physica D* 101:270–288 (1997).
15. T.-S. YANG and T. R. AKYLAS, On asymmetric gravity–capillary solitary waves, *J. Fluid Mech.* 330:215–232 (1997).
16. J. BEALE, Exact solitary water waves with capillary ripples at infinity, *Commun. Pure Appl. Math.* 44:211–257 (1991).
17. J.-M. VANDEN-BROECK, Elevation solitary waves with surface tension, *Phys. Fluids A* 3:2659–2663 (1991).
18. T.-S. YANG and T. R. AKYLAS, Weakly nonlocal gravity–capillary solitary waves, *Phys. Fluids A* 8:1506–1514 (1996).
19. T. R. AKYLAS and R. GRIMSHAW, Solitary internal waves with oscillatory tails, *J. Fluid Mech.* 242:279–298 (1992).
20. T. R. AKYLAS, Envelope solitons with stationary crests, *Phys. Fluids A* 5:789–791 (1993).
21. D. PELINOVSKY, A. SUKHORUKOV, and Y. KIVSHAR, Bifurcations and stability of gap solitons in periodic potentials, *Phys. Rev. E* 70:036618 (2004).
22. G. HWANG, T. R. AKYLAS, and J. YANG, Gap solitons and their linear stability in one-dimensional periodic media, *Physica D* 240:1055–1068 (2011).
23. T. R. AKYLAS, G. HWANG, and J. YANG, From non-local gap solitary waves to bound states in periodic media, *Proc. R. Soc. A* 468:116–135 (2012).

24. S. D. NIXON, T. R. AKYLAS, and J. YANG, Exponential asymptotics for line solitons in two-dimensional periodic potentials, *Stud. Appl. Math.* 131:149–178 (2013).
25. S. D. NIXON and J. YANG, Exponential asymptotics for solitons in \mathcal{PT} -symmetric periodic potentials, *Stud. Appl. Math.* 133:373–397 (2014).
26. J. P. BOYD, *Weakly Nonlocal Solitary Waves and Beyond-All-Orders Asymptotics*, Kluwer, Boston, 1998.
27. T. R. AKYLAS and T.-S. YANG, On short-scale oscillatory tails of long-wave disturbances, *Stud. Appl. Math.* 94:1–20 (1995).
28. O. MORSCH and M. OBERTHALER, Dynamics of Bose–Einstein condensates in optical lattices, *Rev. Mod. Phys.* 78:179–215 (2006).
29. C. C. MEI, Resonant reflection of surface water waves by periodic sandbars, *J. Fluid Mech.* 152:315–335 (1985).
30. R. GRIMSHAW, Exponential asymptotics and generalized solitary waves, in *Asymptotic Methods in Fluid Mechanics: Survey and Recent Advances* (H. Steinrück, Ed.), CISM Courses and Lectures, vol. 523, pp. 71–120, Springer, New York, 2010.

STATE UNIVERSITY OF NEW YORK
MASSACHUSETTS INSTITUTE OF TECHNOLOGY
UNIVERSITY OF VERMONT

(Received February 14, 2017)